Gravity Governs Shear Localization in Confined Dense Granular Flows

M. Reza Shaebani,[1,*] János Török,[2] Maniya Maleki,[3] Mahnoush Madani,[3] Matt Harrington,[4] Allyson Rice,[5] and Wolfgang Losert[6]

[1]Department of Theoretical Physics and Center for Biophysics, Saarland University, 66123 Saarbrücken, Germany
[2]MTA-BME Morphodynamics Research Group, Department of Theoretical Physics, Budapest University of Technology and Economics, Budapest H-1111, Hungary
[3]Department of Physics & Optics Research Center, Institute for Advanced Studies in Basic Sciences, Zanjan 45137-66731, Iran
[4]Department of Physics and Astronomy, University of Pennsylvania, Philadelphia, Pennsylvania 19104, USA
[5]Department of Biophysics Institute, UT Southwestern Medical Center, Dallas, Texas 75390, USA
[6]Department of Physics, University of Maryland, College Park, Maryland 20742, USA

(Received 15 May 2021; revised 10 October 2021; accepted 9 December 2021; published 30 December 2021)

The prediction of flow profiles of slowly sheared granular materials is a major geophysical and industrial challenge. Understanding the role of gravity is particularly important for future planetary exploration in varying gravitational environments. Using the principle of minimization of energy dissipation, and combining experiments and variational analysis, we disentangle the contributions of the gravitational acceleration, confining pressure, and layer thickness on shear strain localization induced by moving fault boundaries at the bottom of a granular layer. The flow profile is independent of the gravity for geometries with a free top surface. However, under a confining pressure or if the sheared layer withstands the weight of the upper layers, increasing gravity promotes the transition from closed shear zones buried in the bulk to open ones that intersect the top surface. We show that the center position and width of the shear zone and the axial angular velocity at the top surface follow universal scaling laws when properly scaled by the gravity, applied pressure, and layer thickness. Our finding that the flow profiles lie on a universal master curve opens the possibility to predict the quasistatic shear flow of granular materials in varying gravitational environments.

DOI: 10.1103/PhysRevLett.127.278003

Superficial layers of many planets and asteroids are covered by granular materials that range in size from dust and sand to gravel and boulder [1]. These layers result from several processes—e.g., volcanic activity, fragmentation, and erosion—and extend to variable depths. Various geological processes occur in near-surface granular layers of celestial bodies. Particularly, shear localization in slow granular flows can initiate catastrophic phenomena such as avalanches, earthquakes, and faulting [2–4]. While the shear strain often localizes in narrow regions near moving boundaries [5,6], the shear zone can also be wide, e.g., when a shear fracture [7] propagates in the bulk away from the boundaries and the sides of the fault move past each other in deep layers—the process that is of particular importance in geology. By pinning the shear band in the bottom of Couette geometries far from the cylinder wall, power-law scalings with the height H of the pile were discovered for the position and width of the shear zone when intersecting the top surface [8,9]. Upon increasing H the shear zone evolves toward the axis of cylinder and eventually undergoes a transition to a closed shear zone buried in the bulk [10–13].

Despite intensive studies on how strain is localized in shear zones [5,6,8–12,14–20], the role of the gravitational acceleration g on the flow profile has remained largely unexplored. Varying g has no obvious effect on localized flow profiles [21,22], but it can influence wide shear zones [23]. Without a constraining top boundary, one expects that g does not affect the shear rheology in rigid-particle systems as it only rescales the pressure gradient [10] (though the stress state and, thus, the flow profile are influenced by g for soft particles [24]). Under a confining pressure, the relative pressure between successive horizontal layers of grains depends on g, suggesting that g alters the shear flow in this case. The shear-zone width was shown to differ when turning on or off g and the external pressure, but the scaling exponent with H remained intact [23]. Although the mechanical behavior of granular matter in low gravity has recently attracted attention [21,22,25–28], it is generally unclear how various geological processes that occur in near-surface granular layers of celestial bodies depend on g. It is crucial to predict the shear flow of granular matter in varying gravitational environments to understand the evolution of planetary and asteroid surfaces and for a successful design of planetary exploration programs and operation of landers, rovers, and subsurface sampling devices.

We combine numerical analysis and experiments to explore the role of g in slow shear flows of granular

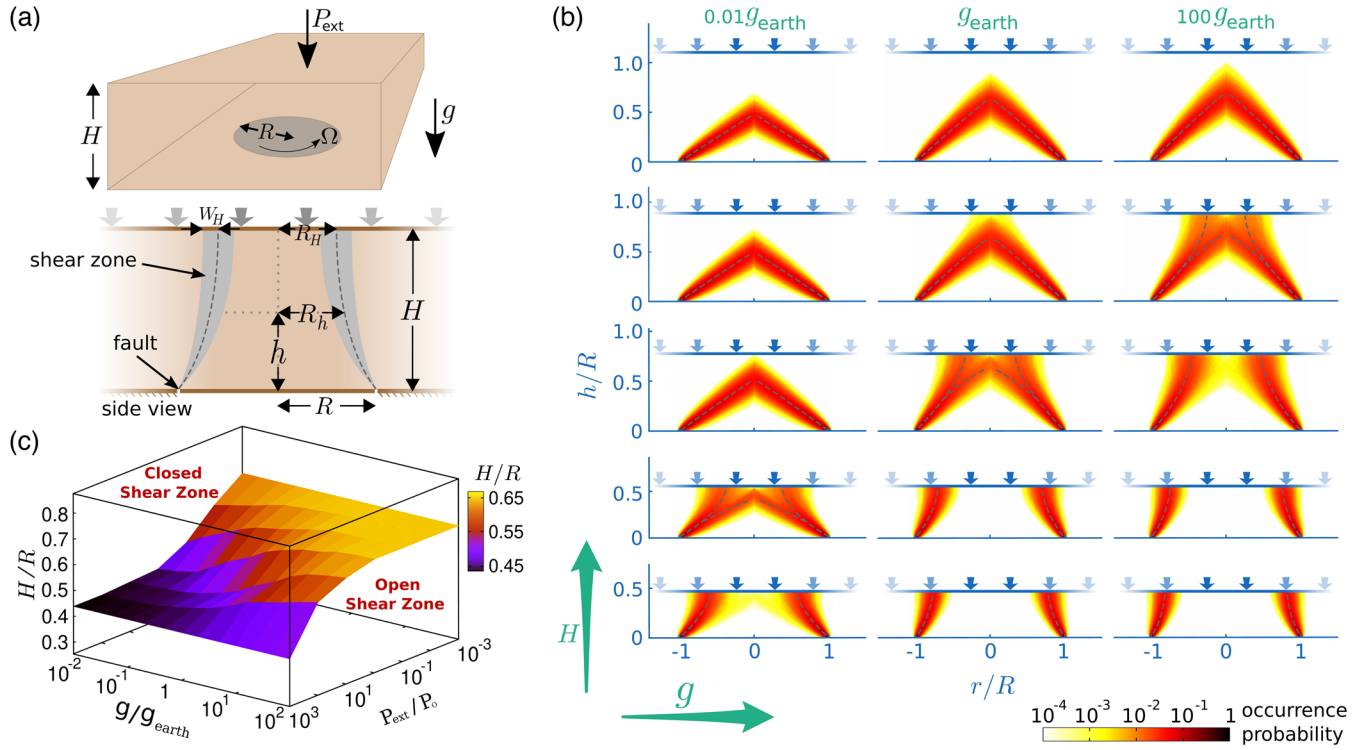

FIG. 1. (a) Sketch of the shear localization zone created by the rotation of a circular region at the bottom of a granular pile. (b) Dependence of the shear-zone type on g and H ($(H/R) = 0.48$, 0.55, 0.77, 0.88, and 1.10 from bottom to top and $g/g_{\text{earth}} = 0.01$, 1 and 100 from left to right. $P_{\text{ext}} = P_\circ$ in all panels. The color identifies the occurrence probability at the given point. The dashed lines mark the center position of the shear zone. (c) Phase diagram of the transition from open to closed shear zones in the (g, P_{ext}, H) space.

materials. We consider a rotating circular fault line at the bottom of a granular layer under confining pressure P_{ext} [Fig. 1(a)] and derive the shape of the shear localization zone from the variational principle of least energy dissipation [10,13]. Increasing g extends the open shear zone regime to thicker layers and pushes the zone away from the axis of rotation while slightly decreasing its width. For closed shear zones, a stronger gravity pulls the shear zone toward the top surface and increases the extent of it. We show that the position and width of the shear zone and the axial angular velocity at the top surface lie on universal master curves when properly scaled by g, H, and P_{ext}. Our experiments in a Couette cell geometry validate the numerical findings.

Shear flow profile from least energy dissipation.—We consider a shear band initiated by a rough disk with radius R rotated at angular velocity Ω at the bottom of a cylindrical granular layer of radius $5R$ and height H [Fig. 1(a)]. We assume that our setup is in the quasistatic regime where inertia effects do not play a role [29] and changing the driving velocity would just change the time scale of the experiment. Thus, the effective friction coefficient is shear-rate independent, which allows one to develop a nonlocal rheology model. We assume the same effective friction coefficient μ in the bulk and near the boundaries; thus, the flow profile is independent of μ (though friction generally plays a major role in stress transmission in granular materials [29–32]). To describe the flow profile, we apply the principle of least dissipation proposed by Onsager for irreversible time-independent phenomena [33–35]. This variational approach has predicted the strain localization path in various sheared granular media accurately [10,13,17,18,36–38].

We require a stationary flow that minimizes the rate of energy dissipation and matches the boundary constraints. Denoting the radial coordinate of the shear band at height h with R_h and taking the cylindrical symmetry of the geometry into account, the variational problem is traced back to finding an optimal R_h function that satisfies $R_0 = R$ while the other boundary at $h = H$ is free. In a narrow shear band approximation [10], the dissipation rate is given by the shear stress $\sigma_{\text{tn}} = \mu[\rho g(H - h) + P_{\text{ext}}]$ times the sliding velocity between the two sides $R_h\Omega$ integrated over the whole shear band. σ_{tn} acts against the sliding direction in the yielding surface, and its magnitude is proportional to μ times the normal component of the stress pressing the two sides against each other. Here we assume that the Janssen effect plays no role and the hydrostatic pressure is applicable. The reason is that the shear band acts as a source of small continuous vibrations in the whole system due to collisions and slip events, which causes a slight creep at contacts [39] and fluidizes the granular bed, inhibiting the

ability of the particles to keep their original anchoring position so that they transmit their load to the next particle below rather than to the side. While the required driving strength depends on g, after the initiation of shearing the hydrostatic pressure holds regardless of the magnitude of g. We present complementary numerical results in the Supplemental Material [40], proving that a realistic stress anisotropy negligibly affects the shear-zone properties of interest. Up to a constant prefactor, the expression to be minimized can be formulated as

$$\int_0^H R_h^2 \sqrt{1+\left(\frac{dR_h}{dh}\right)^2}\left(1-\frac{h}{H}+\frac{P_{\mathrm{ext}}}{\rho g H}\right)dh = \min; \qquad (1)$$

thus, the optimal path is generally determined by g, P_{ext}, H, and R. The optimization procedure leads to an instantaneous narrow shear band. However, the material strength is practically affected in the vicinity of yield events [41], and the resulting random structural changes slightly vary the minimal path in the next instance. In a fluctuating-band version of the model (Supplemental Material [40] and [13]), we consider local fluctuations of the path around the current shear band. While no spatial restriction is imposed by the variational approach on the shear band path, the resulting symmetric shear zone (with respect to the axis of rotation) gains a finite width in the course of such a self-organized process where the global optimum path itself modifies the medium in which the optimization is carried out. The occurrence probability for paths far away from the shear-zone center is practically negligible due to their high energy dissipation cost. The method was previously applied to successfully reproduce the shear-zone width in experiments [13,37]. We obtain the shear profile by ensemble averaging over all instantaneous shear bands calculated via the optimization [Eq. (1)] for a given geometry (H/R) and a set of g and P_{ext} parameters. We checked that the ensemble size of 10^5 is large enough to properly explore the solution space. Note that our minimization approach is indeed a nonlocal process since the material properties are instantaneously modified by the global path (The formalism can be represented in terms of a differential equation similar to Ref. [19]).

Gravity governs the strain localization profile.—We perform extensive numerical simulations based on the optimization scheme to clarify the individual roles of H, g, and P_{ext} on the shear flow profile. g and P_{ext} appear only in the integrand in Eq. (1), but H influences both the integrand and the integral limit.

For a free top surface ($P_{\mathrm{ext}} = 0$), we checked that the flow profile is controlled by (H/R) [8–10]; g plays no role here as it only rescales the contact forces, which does not affect the stress tensor (up to a global prefactor scaling). In contrast, a confining pressure $P_{\mathrm{ext}} \neq 0$ alters the contact forces, microstructure, and dilation behavior of the material [22,24,42–45]. Varying g does not simply rescale the forces; thus, the stress tensor and shear band path depend on both P_{ext} and g parameter values. We choose $P_{\mathrm{ext}} = P_\circ$ ($P_\circ$ being a reference pressure level that a pile of glass beads of size d with height $(H/R) = 0.1$ applies on the bottom disk with $(R/d) = 100$ in the gravitational acceleration of the earth g_{earth}) and vary g by several orders of magnitude at different values of H. As shown in Fig. 1(b), increasing gravity enhances the open shear zone regime to higher values of H. It can be also seen that the gravity pushes the open shear zones away from the axis of rotation and slightly reduces the extent of the zone. This is in contrast to the closed zones, where the gravity even increases the extent of the strain localization zone while pulling it toward the top surface.

The variational approach favors shear zones with relatively small surfaces weighted by the local pressure and sliding velocity. To better understand the role of gravity, we consider two extreme regimes: In a deep layer ($H \gg R$), while a closed shear zone is favorable (as it reduces the total sliding surface), the preferred location of the shear zone is at lower pressure, i.e., higher above the forcing boundary. The competition between these two factors leads to a domelike structure. The strength of gravity determines the optimal height: While the shear zone is a flat disk attached to the bottom plate in the absence of gravity, it changes to a domelike shape when switching on the gravity. By increasing g, the dome gets sharper as shown in the top row of Fig. 1(b). In a very shallow layer ($H \ll R$), an open shear zone is favorable as it requires a relatively smaller surface and benefits from the hydrostatic pressure gradient to reduce the dissipation. While the path is curved toward the axis of rotation to reduce the sliding velocity, increasing g promotes straighter shear zones (i.e., shorter paths) toward the surface to benefit more from the pressure gradient. This effect is obvious in the bottom row of Fig. 1(b). At intermediate H, the interplay of g and P_{ext} is crucial. A typical interface between open and closed shear zones is shown in Fig. 1(c). The transition becomes independent of g and P_{ext} and solely determined by H and R in two extreme cases: When $1 \ll (P_{\mathrm{ext}}/\rho g H)$, the fabric is isotropic under the homogeneous pressure [46], and Eq. (1) reduces to $\int_0^H R_h^2\sqrt{1+(dR_h/dh)^2}dh = \min$, which leads to $h = \int_R^{R_h}[dr/(\sqrt{r^4/A^2-1})]$ by solving the Euler-Lagrange equation (A is a constant). The solution can be expressed in terms of the hypergeometric function ${}_2F_1$ as $h = r\sqrt{r^4/A^2-1}\,{}_2F_1(\frac{3}{4},1;\frac{5}{4};r^4/A^2)$ with the boundary condition $r(h=0) = R$. For $(P_{\mathrm{ext}}/\rho g H) \ll 1$ (as for a layer with a free surface), the strong pressure gradient leads to the variational problem $\int_0^H R_h^2\sqrt{1+(dR_h/dh)^2}[1-(h/H)]dh = \min$ [10], which is again independent of g and P_{ext}.

Universal characteristics of shear zones.—We quantify the center of the shear zone at a given height h as the radial distance R_h at which the rate of the strain reaches its

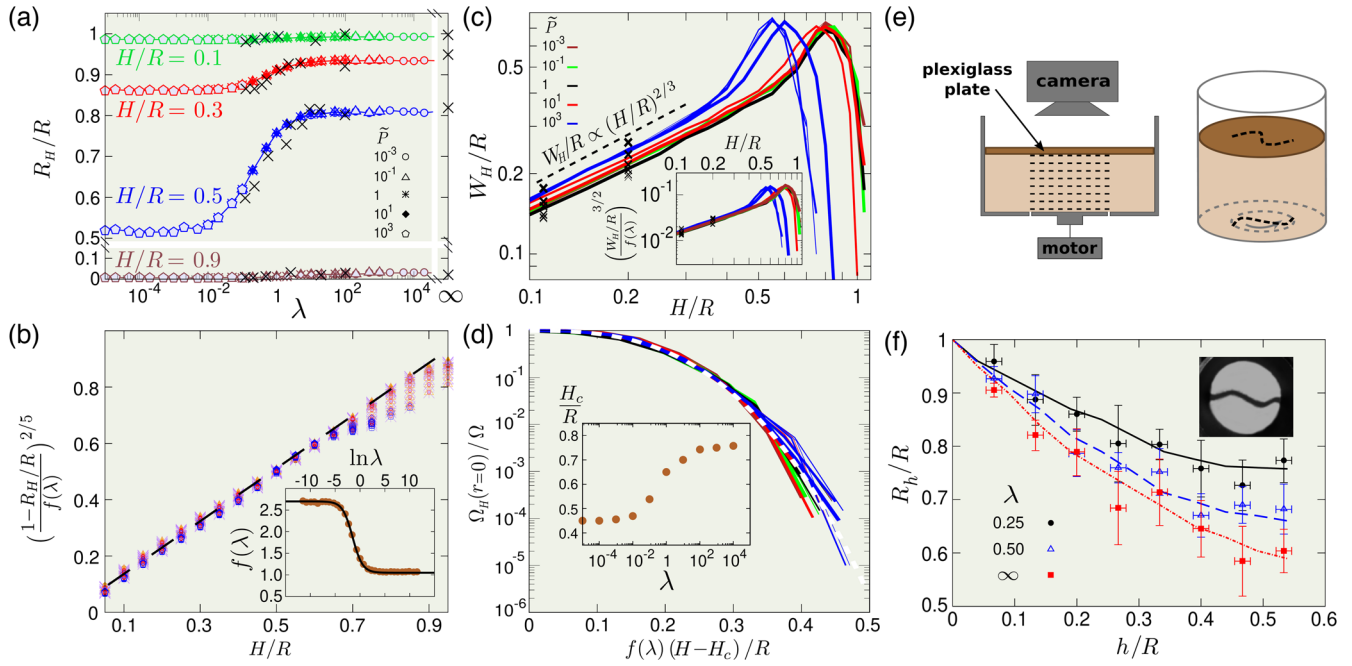

FIG. 2. (a) Collapse of R_H vs λ for all $P_{\rm ext}$ and g values onto a master curve at each H. Crosses denote experimental data. (b) Scaled shear-zone position via Eq. (2) vs (H/R). The dashed line indicates equality. Inset: $f(\lambda)$ vs $\ln\lambda$. The solid line shows a fit to Eq. (3) with $a \simeq 2.7$, $b \simeq -1.7$, $c \simeq 1.5$. (c) W_H vs H for various $P_{\rm ext}$ (different colors) and $g/g_{\rm earth} \in [10^{-2}, 10^{2}]$ (represented with increasing line thickness). Crosses are experimental data at $(H/R) \simeq 0.11, 0.20$ (increasing symbol thickness with $P_{\rm ext}$). Inset: collapse of the data onto a master curve using Eq. (4). (d) $\Omega_H(r=0)$ vs $\tilde{H}$. Same colors and line thicknesses as in panel (c). The white dashed line is the scaling form given by Eq. (5). Inset: cutoff height H_c vs λ. (e) Sketch of the experimental setup and initially straight lines of colored beads within the bulk (left), and evolution of the patterns after shearing (right). (f) R_h vs h, for $(H/R) = 0.55$ and different λ achieved by $(P_{\rm ext}/P_\circ) = 4.0$, 2.0, or 0 in experiments (symbols) or $g/g_{\rm earth} = 0.25$, 0.5, 1 and $(P_{\rm ext}/P_\circ) = 1$, 1, 0 in simulations (lines). The inset shows a typical pattern of colored beads within the bulk, obtained experimentally.

maximum, i.e., $(d\epsilon_{r\theta}/dr)|_{r=R_h} = 0$. The width W_h is taken to be the variance of the shear rate $[d\Omega_h(r)/dr]$ around the peak at $r = R_h$. The behavior of the center position R_H, width W_H, and axial angular velocity $\Omega_H(r=0)$ at the top surface in the (g, H) space is summarized in the Supplemental Material [40], Fig. S1. The transition from open to closed shear bands can be identified as, e.g., when the shear localization region reaches the rotation axis or by the order parameter $m = [\Omega_H(r=0)/\Omega]$ $(m \in [0,1])$ [10–13]. m depends on $P_{\rm ext}$ but approaches a saturation level toward the extreme limits of g; see Supplemental Material [40], Fig. S1(c).

For any choice of H and $P_{\rm ext}$, R_H monotonically increases with g within an H-dependent interval (see Supplemental Material [40], Fig. S2). The growth rate of R_H first increases with g but then decreases. By increasing $P_{\rm ext}$, the position of the maximal growth rate of R_H shifts to larger g values. Denoting the scaled gravity and pressure by $\tilde{g} \equiv (g/g_{\rm earth})$ and $\tilde{P} \equiv (P_{\rm ext}/P_\circ)$, we introduce a control parameter $\lambda = \tilde{g}/\tilde{P}$ with which we tune the relative strength of gravity and applied pressure. When plotting R_H versus λ in Fig. 2(a), the data for all g and $P_{\rm ext}$ values lie on a universal curve at each H, suggesting that to predict the flow profile as a function of gravity, one can instead vary inversely the applied pressure. To validate this hypothesis we carried out shear experiments in a modified Couette cell with a transparent plate on the top of the granular layer to apply pressure [see Fig. 2(e) and Supplemental Material [40] and Ref. [47]]. Figure 2(a) shows that the experimental data obtained by varying the mass of the top plate at different values of H follow the master curves satisfactorily. We achieve a striking data collapse for all g, $P_{\rm ext}$, H, and R_H values on a universal curve

$$1 - \frac{R_H}{R} = f(\lambda)\left(\frac{H}{R}\right)^{5/2}, \tag{2}$$

where $f(\lambda)$ is a logistic function of $\ln\lambda$ [inset of Fig. 2(b)]:

$$f(\lambda) = a + \frac{b}{1 + e^{-(\ln\lambda + c)}}, \tag{3}$$

with a, b, and c being fit parameters. In a free top surface system, $f(\lambda) \approx 1$, and Eq. (2) reduces to a previously reported empirical scaling relation [8,9]. The shear-zone width at the top surface follows a scaling law

$$\frac{W_H}{R} \propto f(\lambda)\left(\frac{H}{R}\right)^{\beta}, \tag{4}$$

with the growth exponent $\beta = 2/3$ [inset of Fig. 2(c)], indicating that the extent of the shear zone grows faster than diffusively but slower than linearly with H (as previously reported in [8,9] and discrete element method simulations of a confined system in the presence or absence of gravity [23]). Note that there are growing deviations from the scaling laws as H approaches the transition threshold to closed shear zones. While the exponent β remains unchanged, increasing (decreasing) g (P_{ext}) slightly decreases W_H, in agreement with DEM simulations [23] and the reported role of gravity on the dispersion of signal width [48].

In shallow layers, the top surface around the axis rotates with the driving rate Ω of the bottom disk. As H increases, $\Omega_H(r=0)$ gradually reduces during the crossover from open to closed shear zones. It can be seen from the inset of Fig. 2(d) that the cutoff height H_c (at which the axial angular velocity at the top surface $\Omega_H(r=0)$ starts decreasing) depends on P_{ext} and g. By subtracting H_c from the total height, we introduce a scaled excess filling height $\tilde{H} = f(\lambda)[(H - H_c)/R]$. Then, the angular velocity data remarkably lie on a universal curve

$$\frac{\Omega_H(r=0)}{\Omega} = \exp\left[-\left(\frac{\tilde{H}}{\sigma}\right)^{\alpha}\right] \tag{5}$$

(with $\alpha \simeq 2.8$ and σ being the standard deviation), which extends over several orders of magnitude.

While the scaling relations [Eqs. (2), (4), and (5)] for the characteristics of the top surface enable one to predict the influence of g on the surface flow profile, the variational approach accurately determines the shear zone path inside the bulk as well. As the final experimental validation of the numerical approach, we first numerically obtain the center position of the shear band in the bulk for a given H and P_{ext} and several choices of g. To achieve the corresponding values of λ in experiments, we adjust P_{ext}, i.e., the mass of the top plate. To be able to visualize the bulk flow profile, we initially create straight lines of colored beads buried at several heights in the bulk and observe the created patterns after shearing by removing the upper layers of grains. The numerical and experimental results of R_h versus h are compared in Fig. 2(f); the agreement is excellent, without any adjustable parameter. We also checked that there is a very good agreement with the previously reported numerical and experimental results for free top surface piles [9,10,49].

In conclusion, we studied the role of gravity on strain localization in slowly sheared granular materials. The variational approach for minimization of energy dissipation is computationally a cheaper technique even compared with efficient DEM tools for large-scale granular simulations [50,51] and can be extended to more complex geometries. We obtained universal scaling laws describing the characteristics of the surface flow profile, which opens the possibility of predicting the shear flow of granular matter in varying gravitational environments. Since shear zones mark the regions where energy dissipation and catastrophic material failures occur, our results are of particular relevance for science and engineering challenges associated with planetary and asteroid exploration programs in the coming years and decades.

J. T. acknowledges support by the Hungarian National Research, Development and Innovation Office (NKFIH), under Grant No. OTKA K 134199, by the BME IE-VIZTKP2020.

*shaebani@lusi.uni-sb.de

[1] D. Hestroffer, P. Sánchez, L. Staron, A. C. Bagatin, S. Eggl, W. Losert, N. Murdoch, E. Opsomer, F. Radjai, D. C. Richardson *et al.*, Astron. Astrophys. Rev. **27**, 6 (2019).
[2] D. R. Scott, Nature (London) **381**, 592 (1996).
[3] A. Daerr and S. Douady, Nature (London) **399**, 241 (1999).
[4] M. Oda and H. Kazama, Géotechnique **48**, 465 (1998).
[5] D. M. Mueth, G. F. Debregeas, G. S. Karczmar, P. J. Eng, S. R. Nagel, and H. M. Jaeger, Nature (London) **406**, 385 (2000).
[6] W. Losert, L. Bocquet, T. C. Lubensky, and J. P. Gollub, Phys. Rev. Lett. **85**, 1428 (2000).
[7] T. I. Riikilä, J. I. Pylväinen, and J. Åström, Phys. Rev. Lett. **119**, 255501 (2017).
[8] D. Fenistein and M. van Hecke, Nature (London) **425**, 256 (2003).
[9] D. Fenistein, J. W. van de Meent, and M. van Hecke, Phys. Rev. Lett. **92**, 094301 (2004).
[10] T. Unger, J. Török, J. Kertész, and D. E. Wolf, Phys. Rev. Lett. **92**, 214301 (2004).
[11] X. Cheng, J. B. Lechman, A. Fernandez-Barbero, G. S. Grest, H. M. Jaeger, G. S. Karczmar, M. E. Möbius, and S. R. Nagel, Phys. Rev. Lett. **96**, 038001 (2006).
[12] D. Fenistein, J.-W. van de Meent, and M. van Hecke, Phys. Rev. Lett. **96**, 118001 (2006).
[13] J. Török, T. Unger, J. Kertész, and D. E. Wolf, Phys. Rev. E **75**, 011305 (2007).
[14] R. R. Hartley and R. P. Behringer, Nature (London) **421**, 928 (2003).
[15] J. E. Kollmer, T. Shreve, J. Claussen, S. Gerth, M. Salamon, N. Uhlmann, M. Schröter, and T. Pöschel, Phys. Rev. Lett. **125**, 048001 (2020).
[16] P. Schall and M. van Hecke, Annu. Rev. Fluid Mech. **42**, 67 (2010).
[17] R. Moosavi, M. R. Shaebani, M. Maleki, J. Török, D. E. Wolf, and W. Losert, Phys. Rev. Lett. **111**, 148301 (2013).
[18] H. A. Knudsen and J. Bergli, Phys. Rev. Lett. **103**, 108301 (2009).
[19] D. L. Henann and K. Kamrin, Proc. Natl. Acad. Sci. U.S.A. **110**, 6730 (2013).
[20] G. Chambon, J. Schmittbuhl, A. Corfdir, J. P. Vilotte, and S. Roux, Phys. Rev. E **68**, 011304 (2003).
[21] N. Murdoch, B. Rozitis, K. Nordstrom, S. F. Green, P. Michel, T.-L. de Lophem, and W. Losert, Phys. Rev. Lett. **110**, 018307 (2013).

[22] N. Murdoch, B. Rozitis, S. F. Green, T.-L. de Lophem, P. Michel, and W. Losert, Granular Matter **15**, 129 (2013).
[23] A. Ries, D. E. Wolf, and T. Unger, Phys. Rev. E **76**, 051301 (2007).
[24] A. Singh, V. Magnanimo, K. Saitoh, and S. Luding, New J. Phys. **17**, 043028 (2015).
[25] K. Harth, T. Trittel, S. Wegner, and R. Stannarius, Phys. Rev. Lett. **120**, 214301 (2018).
[26] A. Sack, M. Heckel, J. E. Kollmer, and T. Pöschel, Granular Matter **17**, 73 (2015).
[27] H. Katsuragi and J. Blum, Phys. Rev. Lett. **121**, 208001 (2018).
[28] M. Noirhomme, A. Cazaubiel, A. Darras, E. Falcon, D. Fischer, Y. Garrabos, C. Lecoutre-Chabot, S. Merminod, E. Opsomer, F. Palencia *et al.*, Europhys. Lett. **123**, 14003 (2018).
[29] G. D. R. MiDi, Eur. Phys. J. E **14**, 341 (2004).
[30] M. R. Shaebani, T. Unger, and J. Kertész, Phys. Rev. E **76**, 030301(R) (2007).
[31] C. Goldenberg and I. Goldhirsch, Nature (London) **435**, 188 (2005).
[32] M. R. Shaebani, T. Unger, and J. Kertész, Phys. Rev. E **79**, 052302 (2009).
[33] L. Onsager, Phys. Rev. **37**, 405 (1931).
[34] L. Onsager, Phys. Rev. **38**, 2265 (1931).
[35] R. Baker and M. Garber, Géotechnique **28**, 395 (1978).
[36] T. Unger, Phys. Rev. Lett. **98**, 018301 (2007).
[37] B. Szabó, J. Török, E. Somfai, S. Wegner, R. Stannarius, A. Böse, G. Rose, F. Angenstein, and T. Börzsönyi, Phys. Rev. E **90**, 032205 (2014).
[38] T. Börzsönyi, T. Unger, and B. Szabó, Phys. Rev. E **80**, 060302(R) (2009).
[39] K. Nichol, A. Zanin, R. Bastien, E. Wandersman, and M. van Hecke, Phys. Rev. Lett. **104**, 078302 (2010).
[40] See Supplemental Material at http://link.aps.org/supplemental/10.1103/PhysRevLett.127.278003 for the details of the fluctuating-band version of the variational approach, the experimental setup, and the behavior of the center position, width, and axial angular velocity at the top surface in terms of the gravitational acceleration and filling height. Furthermore, complementary numerical results are presented to clarify the role of stress anisotropy and particle size on the shear-zone properties.
[41] M. R. Shaebani, T. Unger, and J. Kertész, Phys. Rev. E **78**, 011308 (2008).
[42] M. M. Bandi, P. Das, O. Gendelman, H. G. E. Hentschel, and I. Procaccia, Granular Matter **21**, 40 (2019).
[43] M. Kobayakawa, S. Miyai, T. Tsuji, and T. Tanaka, Phys. Rev. E **98**, 052907 (2018).
[44] M. R. Shaebani, J. Boberski, and D. E. Wolf, Granular Matter **14**, 265 (2012).
[45] P. Das, H. G. E. Hentschel, and I. Procaccia, Phys. Rev. E **99**, 050902(R) (2019).
[46] M. R. Shaebani, T. Unger, and J. Kertész, Int. J. Mod. Phys. C **20**, 847 (2009).
[47] M. Madani, M. Maleki, J. Török, and M. Reza Shaebani, Soft Matter **17**, 1814 (2021).
[48] J. Hong and A. Xu, Phys. Rev. E **63**, 061310 (2001).
[49] A. Singh, V. Magnanimo, K. Saitoh, and S. Luding, Phys. Rev. E **90**, 022202 (2014).
[50] Z. Shojaaee, M. R. Shaebani, L. Brendel, J. Török, and D. E. Wolf, J. Comput. Phys. **231**, 612 (2012).
[51] C. Kloss, C. Goniva, A. Hager, S. Amberger, and S. Pirker, Prog. Comput. Fluid Dyn. **12**, 140 (2012).